Electronic Supplementary Information for

Impact of particle surface chemistry on the structure and rheological properties of graphene-based particle /polydimethylsiloxane composites

Ran Niu,[a,b] Jiang Gong,[a,b] Donghua Xu,[a,*] Tao Tang[a] and Zhao-Yan Sun[a,*]

[a] State Key Laboratory of Polymer Physics and Chemistry, Changchun Institute of Applied Chemistry, Chinese Academy of Sciences, Changchun 130022, P. R. China

[b] University of Chinese Academy of Sciences, Beijing 100039, P. R. China

*To whom correspondence should be addressed.

Tel.: +86 (0) 431 85262896.

Fax: +86 (0) 431 85262969.

E-mail: dhxu@ciac.ac.cn and zysun@ciac.ac.cn

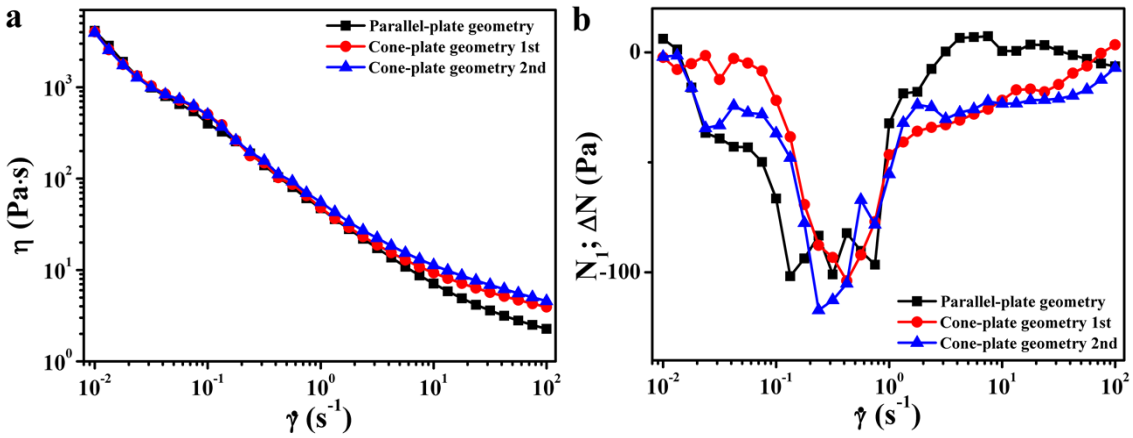

Fig. S1. Viscosity and normal stress differences of 9.1 wt % GP-4/P28 suspension measured by parallel-plate and cone-plate geometries.

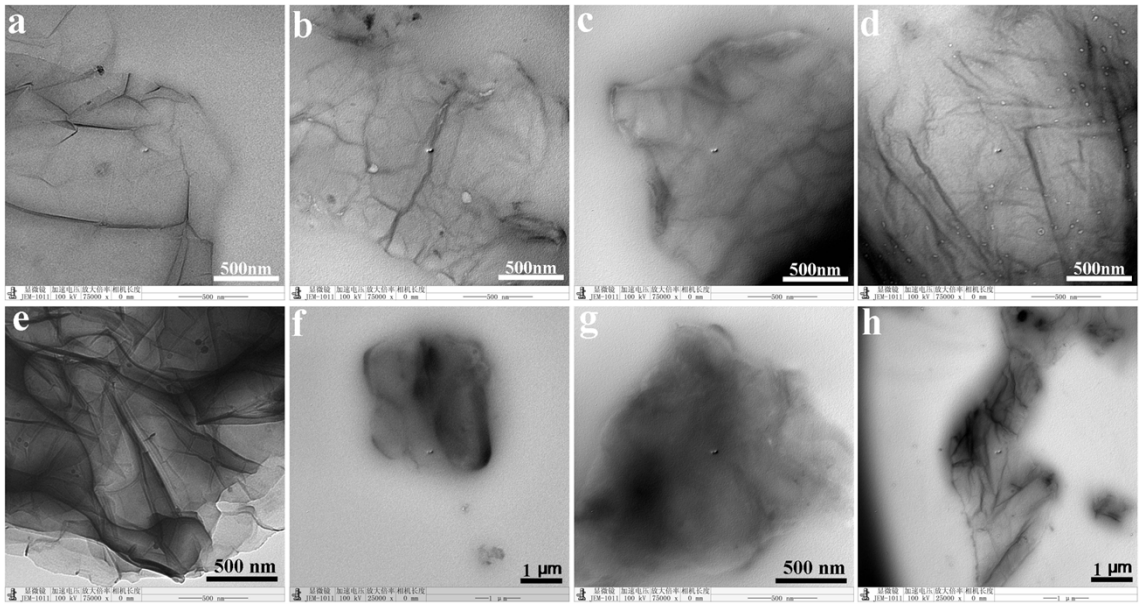

Fig. S2. TEM images of GP-1/P28 (a and e), GP-2/P28 (b and f), GP-3/P28 (c and g) and GP-4/P28 composites (d and h) with 3.7 wt % graphene-based particles.

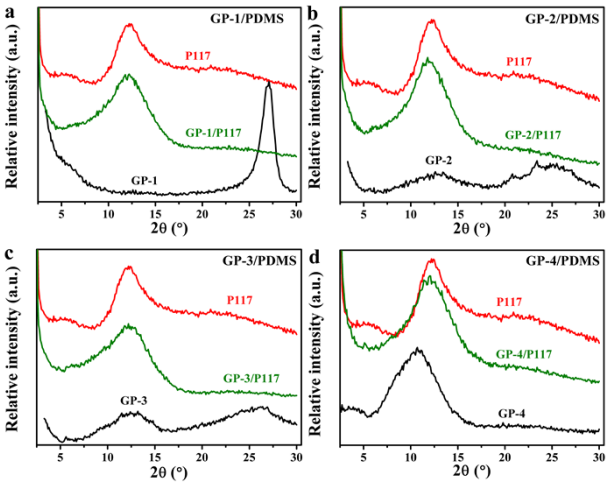

Fig. S3. WAXD patterns of GP-1/P117 (a), GP-2/P117 (b) GP-3/P117 (c) and GP-4/P117 composites (d) with 7.4 wt % graphene-based particles. The curves are vertically shifted for clarity.

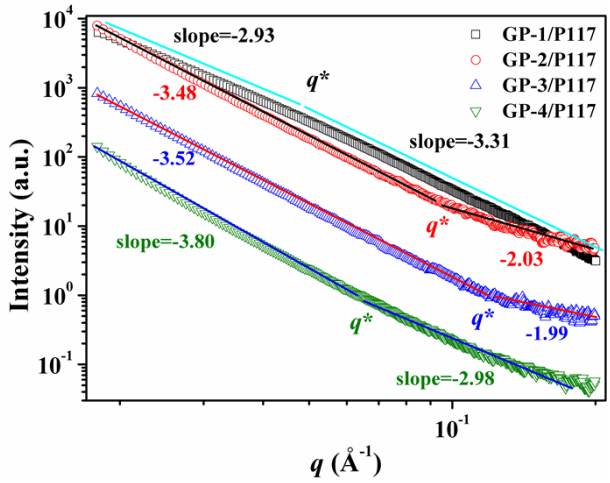

Fig. S4. SAXS profiles of 7.4 wt % graphene-based particle/P117 composites.

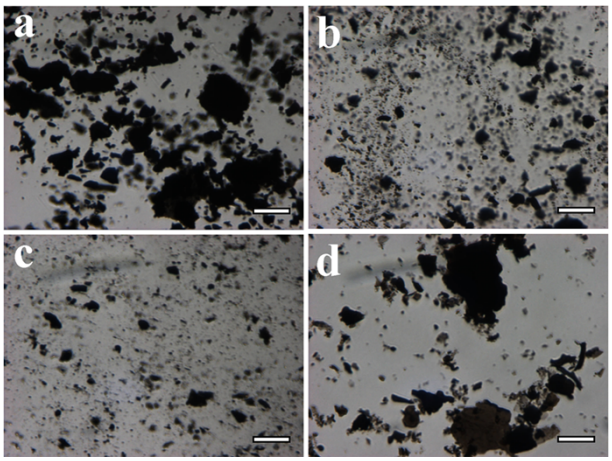

Fig. S5. High resolution optical micrographs of 1.0 wt % graphene-based particle/P28 composites. The scale bars are 30 μm.

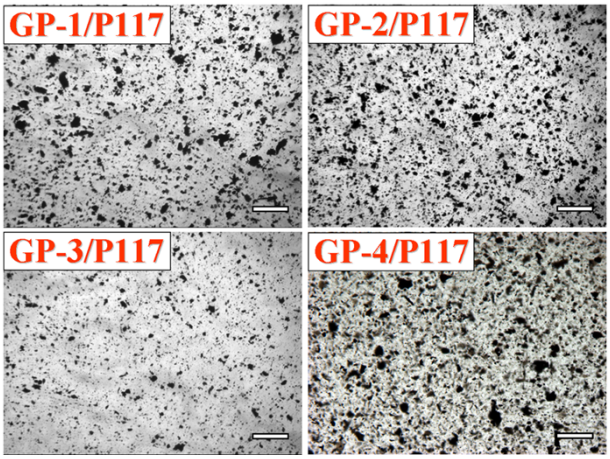

Fig. S6. Optical micrographs of 1.0 wt % graphene-based particle/P117 composites. The scale bars are 150 μm.

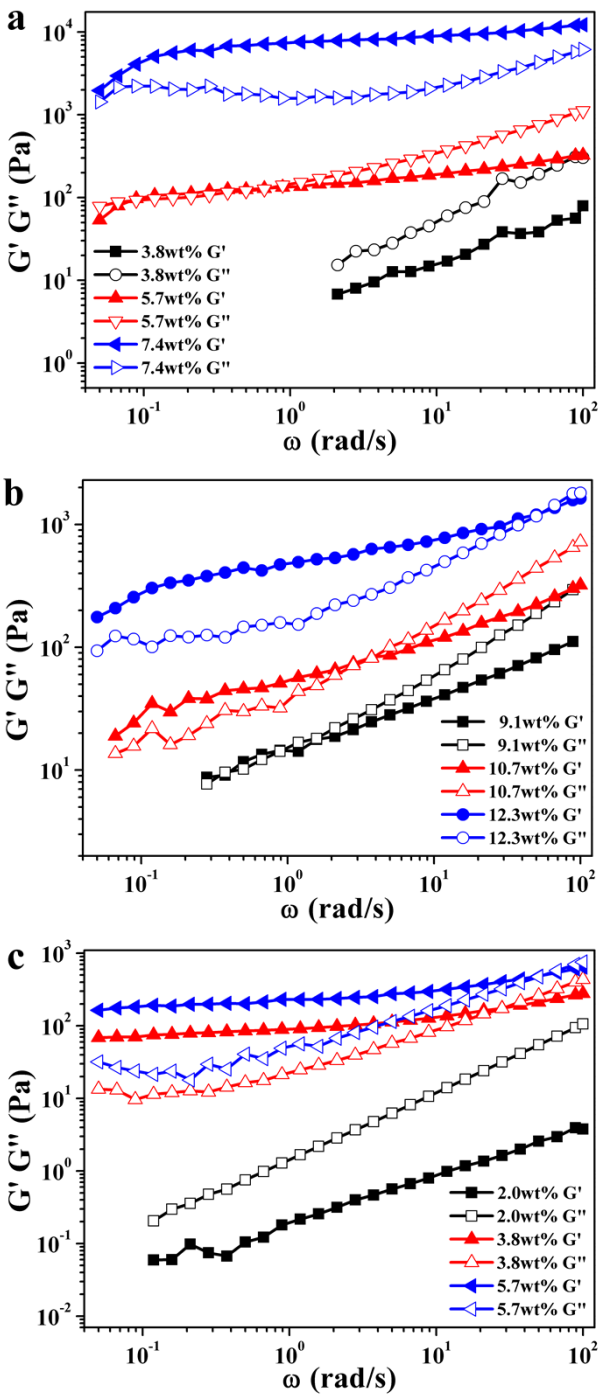

Fig. S7. Frequency sweep results of GP-1/P28 (a), GP-3/P28 (b) and GP-4/P28 composites (c).

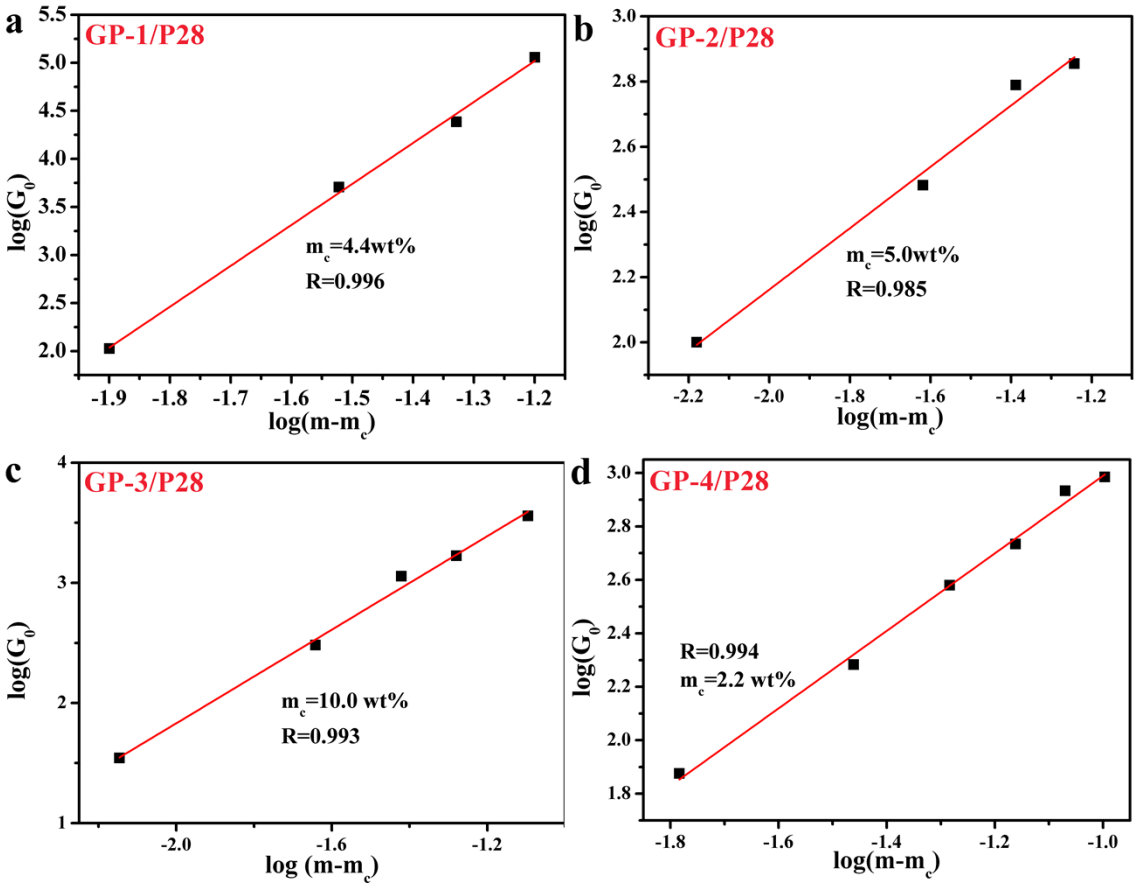

Fig. S8. Log-log plot of plateau modulus versus reduced mass fraction of graphene-based particle/P28 composites.

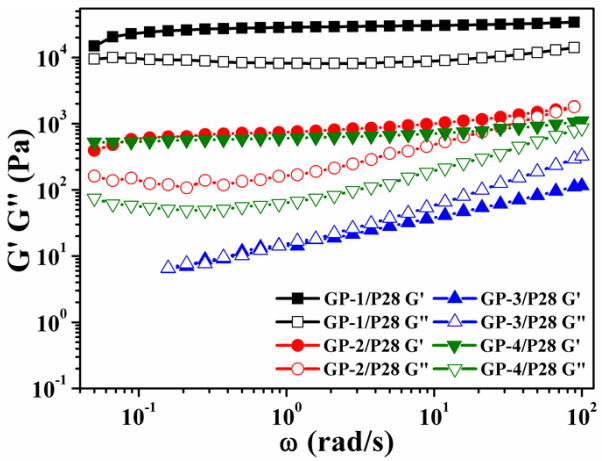

Fig. S9. Storage (G') and loss moduli (G'') versus frequency (ω) for 9.1 wt % graphene-based particle/P28 composites.

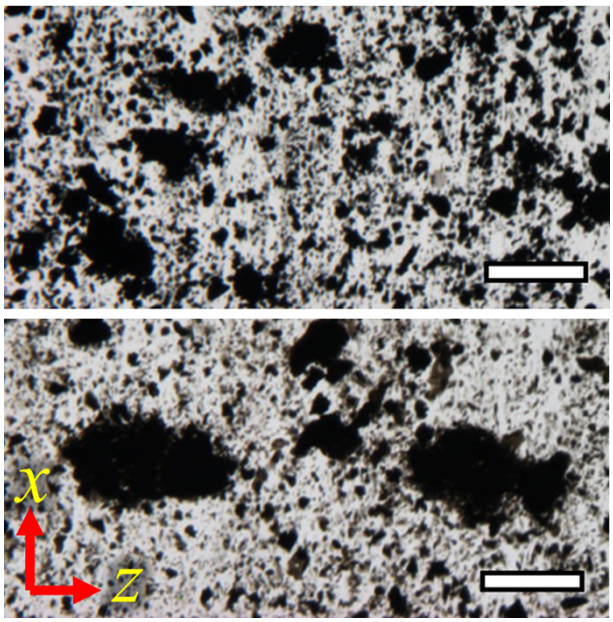

Fig. S10. Detailed micrographs of the vorticity aligned structure of graphene-based particle suspensions. The scale bars are 75 μm.

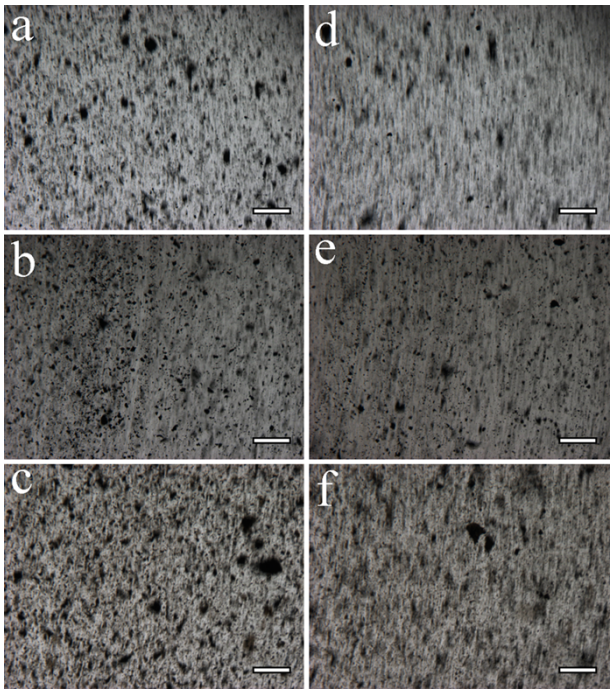

Fig. S11. Structures of 2 wt % GP-2/P28 (a and d), 2 wt % GP-3/P28 (b and e) and 2 wt % GP-4/P28 composites (c and f) under a shear rate of 0.5 s^{-1} (a, b and c) and 1 s^{-1} (d, e and f). The gap is 150 μm and the scale bars are 150 μm. Photos are taken after shearing for about 40 s.

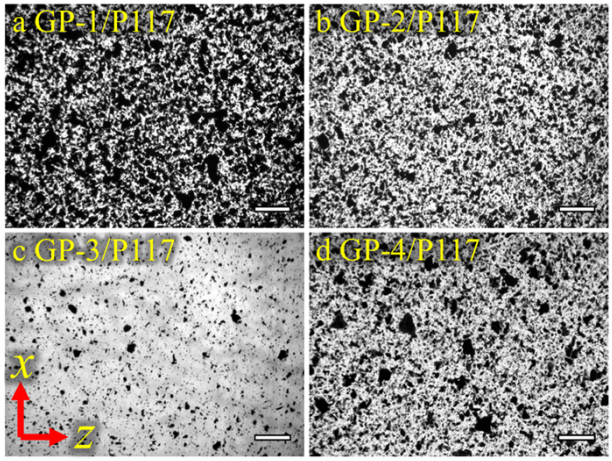

Fig. S12. Structures of 2.0 wt % graphene-based particle/P117 composites at a shear rate of 0.05 s^{-1}. The gap is 150 μm and the scale bars are 150 μm. Photos are taken after shearing for about 40 s.

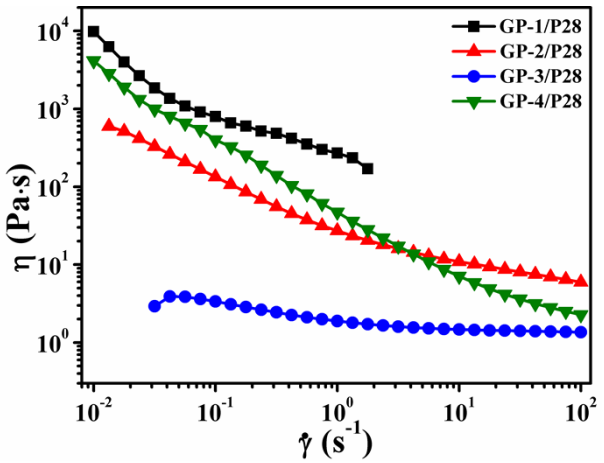

Fig. S13. Viscosity (η) versus shear rate ($\dot{\gamma}$) for 9.1 wt % graphene-based particle/P28 composites.

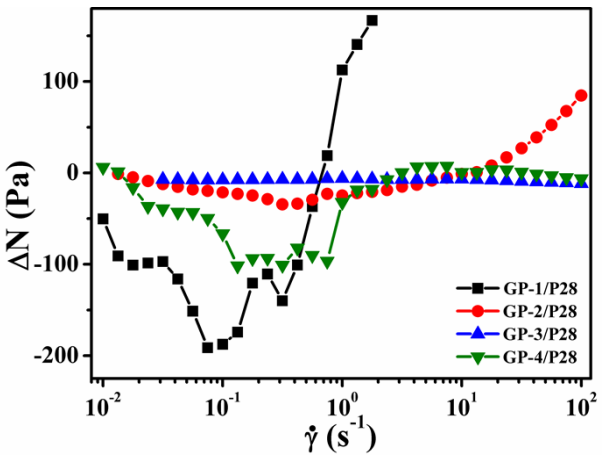

Fig. S14. Normal stress differences (ΔN) versus shear rate for 9.1 wt % graphene-based particle/P28composites.

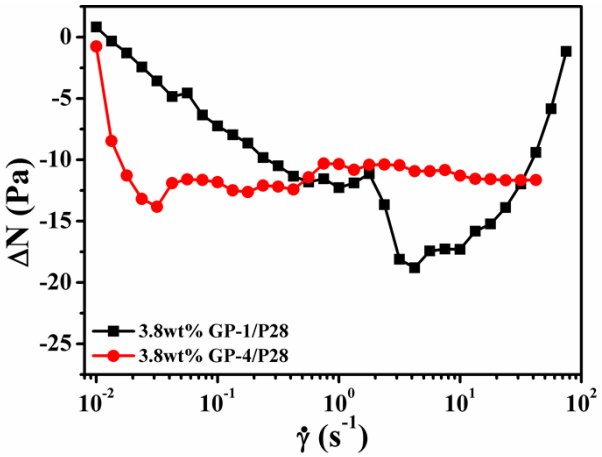

Fig. S15. Normal stress differences (ΔN) versus shear rate for 3.8 wt % GP-1/P28 and 3.8 wt % GP-4/P28 composites.

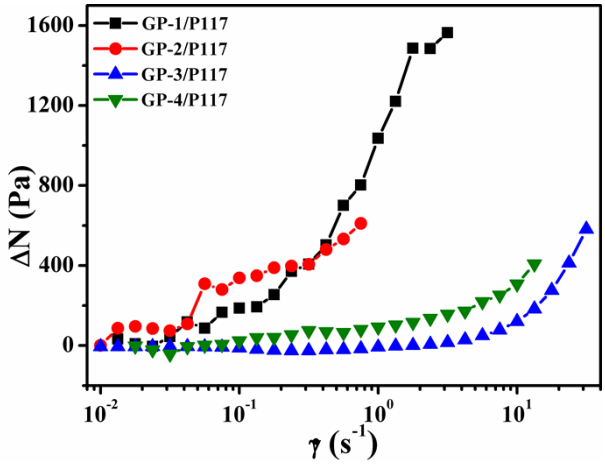

Fig. S16. Normal stress differences (ΔN) versus shear rate for 10.7 wt % graphene-

based particle/P117 composites.

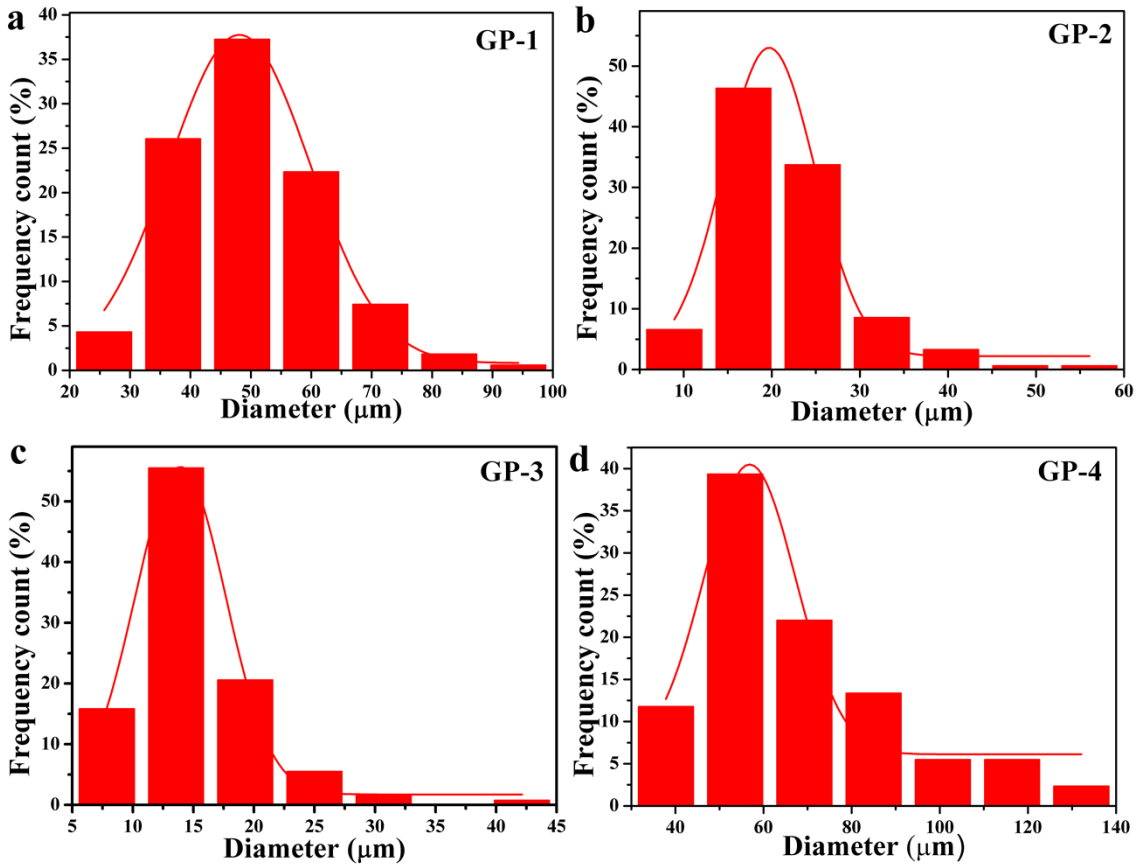

Fig. S17. Diameter distribution and Gaussian fitting of the size of GP-1 (a), GP-2 (b), GP-3 (c) and GP-4 aggregates (d).